

Investigation of the Coordination Chemistry of a Bisamidinate Ferrocene Ligand with Cu, Ag, and Au

Milena Dahlen, Juana Vázquez Quesada,* Luis Santos Correa, Luca Münzfeld, Niklas Reinfandt, Wim Klopper, and Peter W. Roesky*



Cite This: *ACS Omega* 2022, 7, 4683–4693



Read Online

ACCESS |



Metrics & More

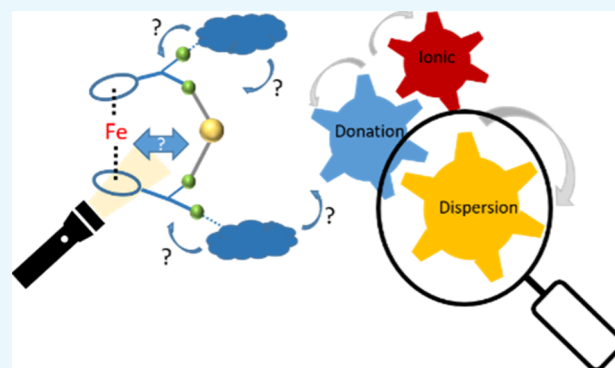


Article Recommendations



Supporting Information

ABSTRACT: The coordination chemistry of a ferrocene ligand with one bulky amidinate function attached to each ring toward two different coinage metal precursors was investigated. In dependence of the metal and the co-ligands, “ansa” type structures and non-bridged structures were obtained. Six different compounds are reported. In the “ansa” type structures, short Fe–M (M = Cu, Ag) distances were observed in the molecular structures in the solid state. However, theoretical calculations (DFT) did not reveal a stabilizing metal–metal interaction. Instead, dispersion interactions within the ligand and between the ligand and metal seem to represent the main stabilization forces.



INTRODUCTION

Ever since the discovery of the first metallocene 7 decades ago, ferrocene has played an important role in different fields of applications.^{1–9} Besides its use as a suitable standard in cyclic voltammetry,¹⁰ as a fuel additive,^{11,12} and others, ferrocene derivatives have caught interest as stable, rigid, and redox-active ligands.^{13–19} Because of the large range of possible ring functionalizations, ferrocene poses a versatile ligand scaffold.^{20,21} One very common choice is the introduction of phosphine groups to ferrocene, which, for example, results in bidentate and sometimes even chiral ligands.²² Depending on the choice of coordination site bound to ferrocene and the metals involved, ferrocene metalloligands may act either as monodentate donors or as multidentate chelating and/or metal bridging ligands.^{23–29} The rich coordination chemistry of ferrocene metalloligands thus mainly depends on the substituents attached to the cyclopentadienyl rings.

Surprisingly, the combination of ferrocene as a versatile ligand scaffold and amidinates, which are a widely used class of ligands for almost all metals of the periodic table ranging from Li to Np,^{30–38} is strongly underdeveloped. Only a few compounds have been reported with amidinate-functionalized ferrocenes so far, and even fewer with disubstituted ferrocenes.^{34,39–43} In coinage metal chemistry, amidinates tend to coordinate in a metal bridging mode, forming an {(amidinate)₂(amidinate)} metal core (Figure 1, left) if weakly bound leaving groups are coordinated to the metal precursor. Otherwise, a κ^1 -structural motif is seen (Figure 1, right). By using ferrocene-1,1'-diyl-functionalized bis(amidinates) as ligands, one would expect the formation of metallopolymers (Figure 1). We employed very

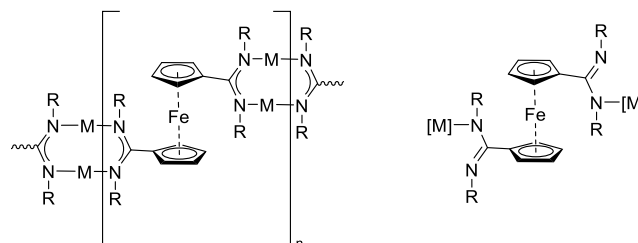


Figure 1. Schematic drawing of the two mentioned structural motives. Left: polymeric structure; right: κ^1 -mode.

bulky substituted amidinates as functional groups in order to break the “normal” coordination modes, which lead to polymers. Note that it should be kept in mind that Cu(II), Ag(I), and Au(I) precursors may potentially oxidize ferrocene to ferrocenium.^{44,45}

Herein, we report the application of a ferrocenyl bis-(amidinate) with the bulky substituent 2,6-diisopropylphenyl (DIPP) on the nitrogen atoms as a ligand in coinage metal chemistry.^{46–49} By combining theory and experiments, we aim at shedding light on the bonding situations of the obtained complexes. This work might be useful to provide insights into

Received: December 13, 2021

Accepted: January 10, 2022

Published: January 25, 2022

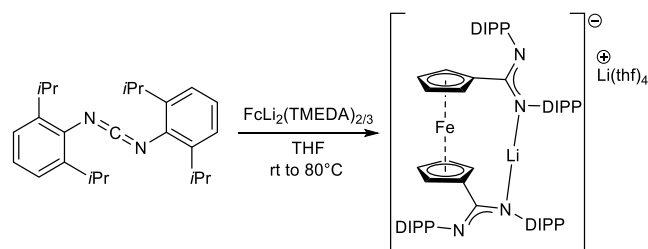


the influence of the ligand on assumed iron–metal interactions, being a crucial part in synthesizing and understanding redox-switchable devices for applications in luminescence or catalysis.

RESULTS AND DISCUSSION⁵⁰

Ligand Synthesis. Following an adapted literature procedure, the ligand precursor $[\text{Fc}(\text{NCN}^{\text{DIPP}})_2\text{Li}][\text{Li}(\text{thf})_4]$ (**1**) was synthesized from the dilithioferrocene tetramethylethylenediamine (TMEDA) adduct $[\text{FcLi}_2(\text{TMEDA})_{2/3}]$ and bis(2,6-diisopropylphenyl) carbodiimide (Scheme 1).³⁴ After dissolving both reactants in hot THF and letting the orange-red solution cool down to room temperature, **1** was isolated as an orange crystalline material (yield 34–70%).

Scheme 1. Synthesis of the Proligand
 $[\text{Fc}(\text{NCN}^{\text{DIPP}})_2\text{Li}][\text{Li}(\text{thf})_4]$ (**1**)



Single X-ray diffraction studies revealed an “ansa” type motif similar to that of its published mesityl analogue (Figure 2).³⁴ The lithium atom Li1 in the main motif is coordinated by one nitrogen atom of each amidinate unit in a bent linear coordination ($\text{N}2\text{--Li}1\text{--N}3$ $164.8(3)^\circ$). The second lithium

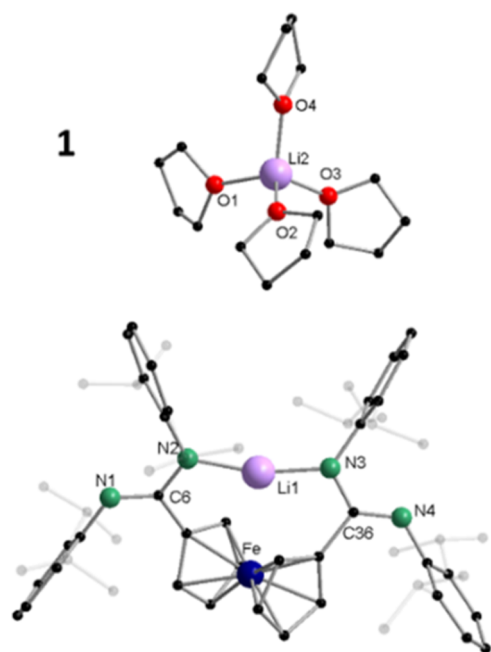


Figure 2. Molecular structure of proligand **1** in the solid state. Hydrogen atoms are omitted for better visibility. Selected bond lengths [Å] and angles [$^\circ$]: $\text{N}2\text{--Li}1$ 1.931(5), $\text{N}3\text{--Li}1$ 1.925(5), $\text{N}1\text{--C}6$ 1.309(4), $\text{N}2\text{--C}6$ 1.338(4), $\text{N}3\text{--C}36$ 1.339(4), $\text{N}4\text{--C}36$ 1.307(3), $\text{O}1\text{--Li}2$ 1.927(8), $\text{O}2\text{--Li}2$ 1.945(9), $\text{O}3\text{--Li}2$ 1.925(9), $\text{O}4\text{--Li}2$ 1.922(8), $\text{N}3\text{--Li}1\text{--N}2$ $164.8(3)$, $\text{N}1\text{--C}6\text{--N}2$ $124.5(3)$, $\text{N}4\text{--C}36\text{--N}3$ $124.2(3)$.

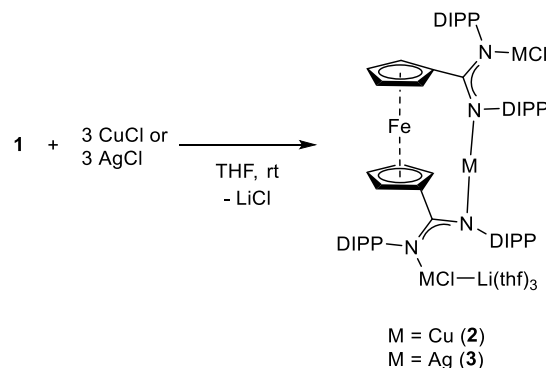
atom is separated from the main motif and forms the solvated $[\text{Li}(\text{thf})_4]^+$ counteranion. Other than in the previously reported structure,³⁴ there is no additional THF molecule coordinated on Li1, probably due to the larger steric demand of the DIPP substituents. Similar C–N bond lengths within each N–C–N unit indicate delocalization of the negative charge between the nitrogen atoms. Ferrocene cyclopentadienyl (Cp) rings in **1** show a tilt angle ($\text{Cp}\text{--Fe}\text{--Cp}'$) of 8.71° and are twisted against each other by 66.0° [Table S3, Torsion (Am)] in the amidinate substituents (see Figure S40 for definition of the tilt and torsion angles).

Noteworthy, the iron and lithium atoms are far closer ($\text{Fe}\text{--Li}1$ 2.845(5) Å) than previously reported ($\text{Fe}\text{--Li}$ 3.732 Å).³⁴

The best results for NMR spectroscopy were obtained in $\text{DMSO-}d_6$ due to possibly hindered rotation. However, **1** is only stable for a very limited time in DMSO, so NMR analytics was complemented by measurements in $\text{THF-}d_8$. Dynamic behavior at room temperature necessitated low-temperature NMR spectroscopy. Upon cooling down to 213 K, resonances sharpened significantly and allowed identification of different proton groups.

Complexes from Coinage Metal Chlorides. We first chose to react **1** with the coinage metal chlorides (Scheme 2).

Scheme 2. Synthesis of Trinuclear Complexes 2 and 3
(Nuclearity Refers to Coinage Metal Loading)



Initially, two equivalents of the metal precursor were used. However, the trinuclear complexes (nuclearity refers to coinage metal loading) $[\text{Fc}(\text{NCN}^{\text{DIPP}})_2\text{Cu}(\text{CuCl})_2\text{Li}(\text{thf})_3]$ (**2**) and $[\text{Fc}(\text{NCN}^{\text{DIPP}})_2\text{Ag}(\text{AgCl})_2\text{Li}(\text{thf})_3]$ (**3**) were obtained. The observed trimetallic structural motif is unprecedented for amidinates. In each complex, two coinage metals are linearly coordinated each by one nitrogen atom from one amidinate unit and one chlorine atom. The third coinage metal atom bridges both amidinate units and thus forms an “ansa” type structural motif. While this type of coordination motif is known for the alkaline metals,³⁴ it is to our knowledge unknown for the coinage metals. The unusual coordination might be a result of the bulky DIPP substituents of the amidinate nitrogen atoms. These prevent the formation of a $\{(\text{amidinate})\text{M}_2(\text{amidinate})\}$ metal core (Figure 1).

After reaction in THF and crystallization from THF/*n*-pentane, copper complex **2** was isolated as orange crystals (yield 21%). Single-crystal diffraction revealed that Cu2 is nearly linearly coordinated by each one nitrogen atom of different amidinate substituents [$\text{N}3\text{--Cu}2\text{--N}2$ $177.64(11)^\circ$] (Figure 3). Additionally, each amidinate unit carries one copper chloride moiety in a bent linear arrangement [$\text{N}1\text{--Cu}1\text{--Cl}2$ $166.32(9)^\circ$ and $\text{N}4\text{--Cu}3\text{A}\text{--Cl}1\text{A}$ $167.87(12)^\circ$, latter disordered by 15%,

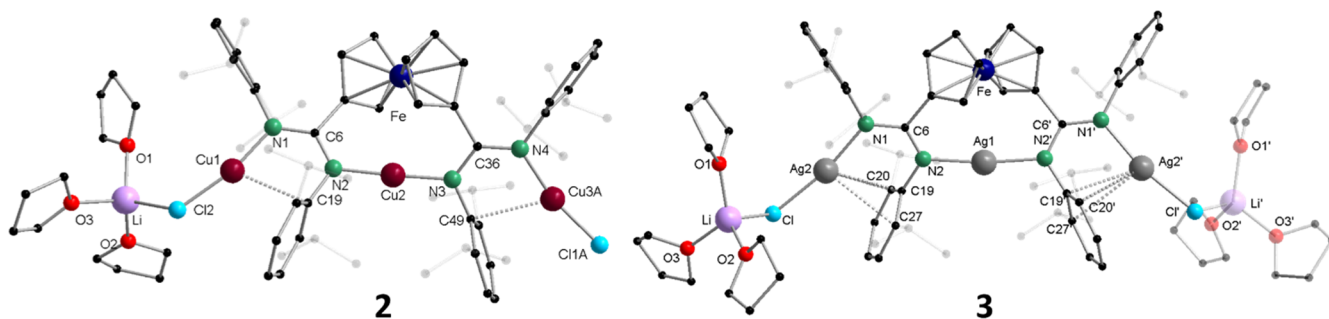


Figure 3. Molecular structures of copper complex **2** and silver complex **3** in the solid state. Hydrogen atoms are omitted for better visibility. Selected bond lengths [Å] and angles [°]: **2**: Cu1–N1 1.888(3), Cu2–N2 1.872(3), Cu2–N3 1.865(3), Cu3A–N4 1.935(3), N4–Cu3B 1.778(11), Cu1–Cl2 2.1141(10), Cu3A–Cl1A 2.129(2), N1–C6 1.332(4), N2–C6 1.329(4), N3–C36 1.337(4), N4–C36 1.325(4), N3–Cu2–N2 177.64(11), N1–Cu1–Cl2 166.32(9), N4–Cu3A–Cl1A 167.87(12), N2–C6–N1 123.9(3), N4–C36–N3 122.6(3). The Cu1–Cl1 unit is disordered by 15% (not displayed). **3**: Ag1–Fe1 3.1504(5), Ag1–N2 2.066(2), Ag2–N1 2.135(2), Ag2–Cl1 2.3376(6), N1–C6 1.328(3), N2–C6 1.330(3), N2–Ag1–N2' 172.90(10), N1–Ag2–Cl1 168.85(5), N1–C6–N2 123.1(2). Note: the Li(thf)₃ moiety of **3** is half occupied.

only main part A is discussed]. Coordination of a {Li(thf)₃}⁺ moiety to Cl2 leads to an overall neutral complex. Close distances between the metal atoms Cu1 and Cu3A and neighboring carbon atoms [C^{Ar}–Cu (**2**): 2.656(4) Å, 2.663(3) Å] indicate an additional stabilizing metal- π interaction (C^{Ar} = carbon atom of the phenyl ring, see Figure 3, dotted line).^{51,52}

A rather short distance of 3.1154(6) Å between iron and copper (Cu2) was found. This value is slightly longer than the reported Cu–Fe distance from Struchkov (2.945 Å) and shorter than the sum of the van der Waals radii determined by Batsanov (4.05 Å).^{53–55} To understand these contacts, theoretical investigations were performed, which are discussed below. As for **1**, the N–C–N bond lengths are roughly the same, indicating a charge delocalization between the nitrogen atoms. Both the torsion angle between amidinate substituents (69.0°) and the tilt angle of the Cp rings (6.71°) are also similar to those of **1**.

Owing to its low solubility and dynamics in solution, NMR spectra were difficult to obtain. However, compound **2** was unambiguously identified via elemental analysis and mass spectrometry [$m/z = 1169.267$ ([M–Li(thf)₃][–] calc. 1169.266)].

Analogous to **2**, the obtained silver complex **3** was isolated as an orange light-sensitive crystalline material (yield 26%). Complex **3** is otherwise very similar to **2**, also featuring the central metal atom Ag1 in a bridging position which is nearly linearly coordinated by N2 and N2' (172.90(10)°). Adjacent to N1, an [AgClLi(thf)₃]⁺ moiety is coordinated with Li(thf)₃, being only half occupied (this half occupied symmetric structure is represented in Figure 3 through two Li(thf)₃ groups being one of the quasi-transparent).

As for **2**, close contacts between Ag2 and neighboring carbon atoms [C^{Ar}–Ag (**3**): 2.742(2) Å, 3.002(2) Å, 3.064(2) Å] indicate a metal- π interaction.⁵² The amidinate angles remain for **2** and **3** basically unchanged. Despite the similarities, some differences are to be mentioned. Probably owing to the larger ion radius of silver, the tilt angle of the Cp rings is double the value as in **2** (11.9°), while the torsion angle between the amidinate groups remains basically unchanged (68.5°). The intermetallic Fe–Ag distance counts for 3.1506(6) Å, which is only minor longer than in a complex from Sazonova (3.0909(7) Å) and significantly shorter than the sum of their van-der-Waals radii (4.15 Å, Batsanov).^{54–56}

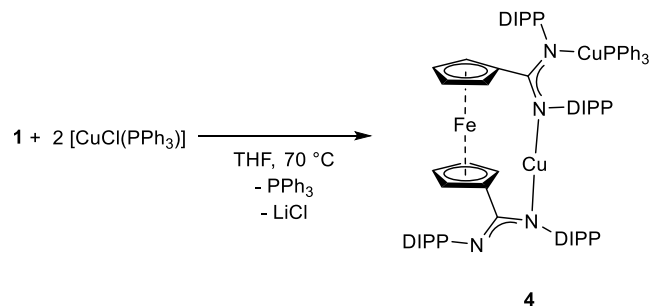
Compound **3** shows only limited stability during crystallization in its mother liquor and remains after crystallization

either insoluble or instable in organic solvents so that NMR spectroscopy is not practicable.

Reaction with [AuCl(tht)] (tht = tetrahydrothiophene) to generate the respective gold complex was not successful and led under various conditions to decomposed unidentified products, probably containing elemental gold (black and/or purple precipitate).

Complexes from Triphenylphosphine Metal Chlorides. Next, we reacted **1** with group 11 triphenylphosphine metal chlorides [MCl(PPh₃)] (M = Cu, Ag, Au) in a 1:2 ratio (Scheme 3 and Scheme 4). We intended to assess the influence

Scheme 3. Synthesis of the Binuclear Copper Complex **4** (Nuclearity Refers to Coinage Metal Loading)



of the co-ligand compared to chlorine and whether it leads again to “ansa” type structural motives or to a κ^1 -mode (Figure 1, right). In general, one would expect the formation κ^1 -N-coordinated {M(PPh₃)₃}⁺ complex fragments. Single crystals of the copper complex [Fc(NCN^{DIPP})₂Cu(CuPPh₃)] (**4**) were obtained from crystallization in THF/*n*-pentane (gas diffusion). The quality of the obtained X-ray structural data set does not allow detailed structure discussion, and only atom connectivity could be confirmed. Elemental composition was validated by electrospray ionization–high-resolution mass spectrometry (ESI–HRMS).

As seen for **2** and **3**, an “ansa” type structural motif is formed in **4**. However, in this case, only two copper atoms are incorporated. During the course of reaction, loss of one PPh₃ moiety occurs (Figure 4).

Obviously, the {Cl–Li(thf)₃} moiety, which stabilizes the coordination sphere of the outer copper atoms (Cu1) in **2**, is not formed in **4**. In **4**, the central copper atom is again linearly coordinated by N2 and N3, while the second Cu2 is coordinated

Scheme 4. Synthesis of the Binuclear Silver and Gold Complexes 5 and 6 (Nuclearity Refers to Coinage Metal Loading)

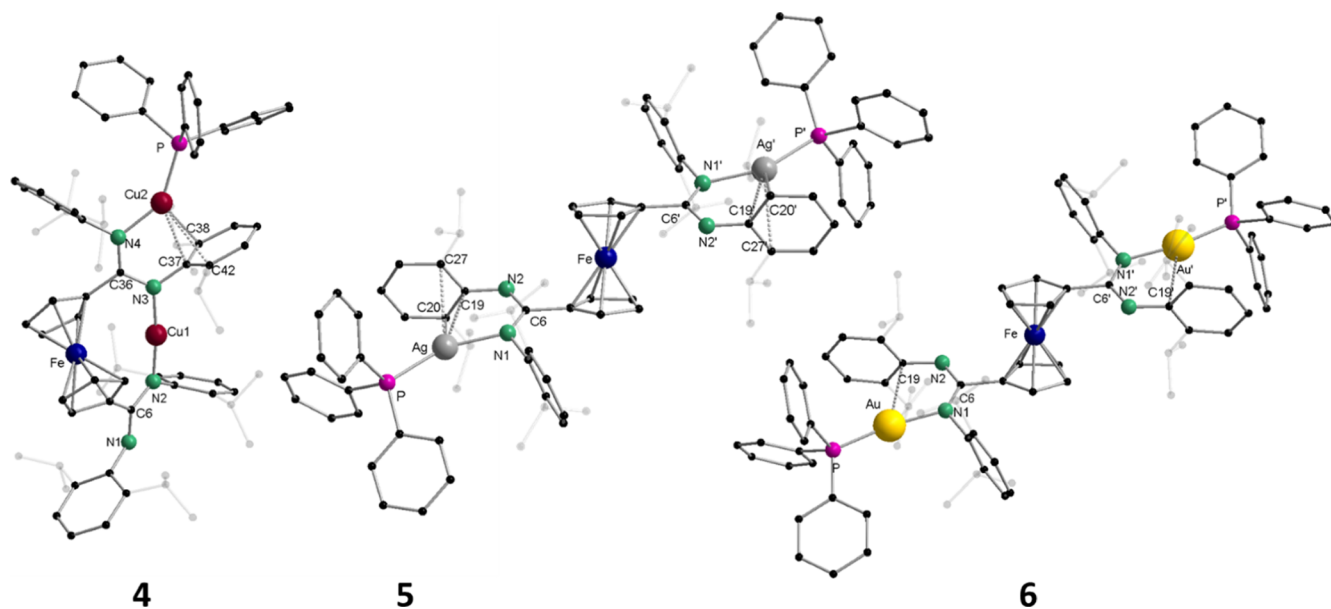
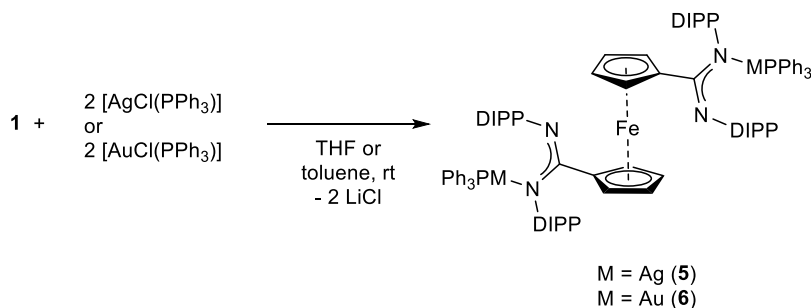


Figure 4. Molecular structures of copper complex **4**, silver complex **5**, and gold compound **6** in the solid state. Hydrogen atoms and non-coordinating solvent molecules are omitted for better visibility. Selected bond lengths [Å] and angles [°]: **5**: Ag–P 2.3250(8), Ag–N1 2.117(2), Ag–C19 2.683(3), N1–C6 1.337(4), N2–C6 1.318(4), N1–Ag–P 153.64(6), N2–C6–N1 123.6(2). **6**: Au–P 2.2311(14), Au–N1 2.057(4), N1–C6 1.348(6), N2–C6 1.299(6), N1–Au–P 167.74(12), N2–C6–N1 126.3(5).

by N4 and a triphenyl phosphine moiety. However, this behavior is in accordance with Pearson's HSAB principle.^{57,58} From the obtained data, the tilt angle of **4** was determined to be $\sim 4.2^\circ$ and the torsion angle was determined to be $\sim 72^\circ$, both being in the same range as for **2**. $^{31}\text{P}\{^1\text{H}\}$ NMR spectroscopy revealed a single phosphorus resonance at $\delta = 8.3$ ppm. ^1H resonances could be assigned by recording ^1H and COSY spectra down to 223 K (dynamic behavior at room temperature). The molecular composition was further validated by HRMS.

Conversely, reactions with the respective heavier homologues silver and gold gave the expected $\kappa^1\text{-N}$ amidinate coordination.

The synthesis of $[\text{Fc}(\text{NCN}^{\text{DIPP}}\text{AgPPh}_3)_2]$ (**5**) occurred in THF with subsequent crystallization from THF/*n*-pentane in 53% yield. The reaction solution of **5** is temperature- and light-sensitive. Single-crystal X-ray diffraction analysis reveals a symmetric structure with both $\{\text{Ag-PPh}_3\}^+$ moieties being exactly opposite of each other and a torsion angle of 180° (Figure 4). The Cp rings are perfectly planar (tilt angle 0°) and in staggered conformation. The silver cations are in a bent linear coordination environment by one nitrogen and one phosphorus atom (N1–Ag–P 153.64(6)). The NCN angle in **5** is somewhat wider than in **2** and **3** but smaller than in **1**. $^{31}\text{P}\{^1\text{H}\}$ NMR spectroscopy reveals one resonance at $\delta = 15.7$ ppm appearing as

two doublets from coupling of the ^{31}P nucleus with both ^{107}Ag and ^{109}Ag nuclei ($J_{\text{P},^{109}\text{Ag}} = 667.8$ Hz and $J_{\text{P},^{107}\text{Ag}} = 578.3$ Hz).

The respective gold compound $[\text{Fc}(\text{NCN}^{\text{DIPP}}\text{AuPPh}_3)_2]$ (**6**) was obtained from reaction of **1** with $[\text{AuCl}(\text{PPh}_3)]$ in toluene at room temperature and crystallization from toluene/*n*-pentane (crystalline yield 28%). Although **6** is easily reproducible, it was not possible to isolate it in an analytic pure form. In addition to the co-crystallization of the starting material $[\text{AuCl}(\text{PPh}_3)]$, which could not be prevented even by different reaction conditions, $^{31}\text{P}\{^1\text{H}\}$ NMR spectroscopy reveals several different signals in solution. This indicates a not clean formation and a lower stability of **6** in solution. For this reason and because of its low solubility, NMR spectroscopy for **6** proved to be difficult and only the solid-state structure is discussed below. However, this is consistent with the observations from the reactions with the coinage metal chlorides, where the Au species was also the least stable and therefore not accessible.

The molecular structure of **6** in the solid state shows the same molecular conformation as in **5** with opposite orientation of the N–Au–PPh₃ moieties and staggered co-planar Cp ring conformation (Figure 4). The observed N–Au–P angle is less bent than the respective angle in **5** and was determined to be $167.74(12)^\circ$.

All three compounds, **4**, **5**, and **6** show again short M–C distances to neighboring phenyl groups [(C^{Ar}–Cu (**4**): 2.401–2.756 Å; C^{Ar}–Ag (**5**): 2.683(3)–2.950(3) Å; C^{Ar}–Au (**6**): 2.976(5) Å], indicating π -metal stabilization.⁵² While for copper, the “ansa” type motif is observed in **4**, this was not the case for Ag and Au. However, this might be due to the “harder” character of the Cu⁺ ion. Probably, the coordination of two anionic nitrogen atoms to the copper atom is favored compared to the mixed N–Cu–P coordination.

Both structural motives are summarized in Figure 5. The formation of the unexpected “ansa” type structure is shown in

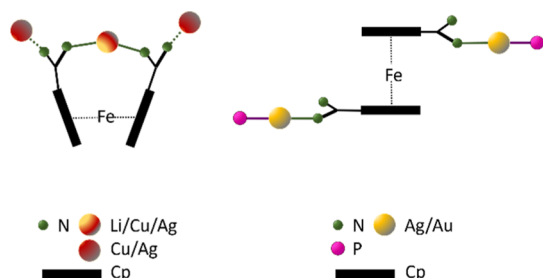


Figure 5. Schematic drawing of the two structural motives obtained. Left: “ansa” type structure with possible Fe–M interaction; right: open form.

Figure 5 (left), while the expected open form is shown on the right hand side of Figure 5. For understanding the differences in the formation of the structures and for getting an insight in the Fe–M interactions in the “ansa” type complexes, theoretical investigations were performed.

Theoretical Section. Among the different criteria discussed in the literature to identify Fe–M interactions, one of the first considered is the distance between the metal (M) and Fe in comparison to the sum of the corresponding van der Waals radii. In the case of ferrocene, other criteria have been extensively discussed in the past. Among them is the angle of inclination between the two cyclopentadienyl rings (Cp–Cp’), the so-called tilt angle, as well as other structural parameters that indicate a distortion of the eclipsed configuration of the ferrocene group (D_{5h}).^{23,59,60} Although it is expected that the angle of inclination between the two rings (Cp–Cp’) increases with the size of the metal, high values of this angle also indicate the proximity between Fe and M and with it, what has been classically described as electron-donating abilities of the Fe center.^{23,26,61–63} In this work, we investigate all these aspects in conjunction with other structural parameters (see Figure S40) as well as the quantification of long-range dispersion interactions that also influence not only the interaction between Fe and M but also the interactions of other metals present in the molecule (M’) with the DIPP-groups, which can play a decisive role in the

stabilization of the complexes that are object of this study. The experimentally determined structural parameters as well as those obtained using different density functional theory (DFT) models for the main motif of **1** (anion [Fc(NCN^{DIPP})₂Li][−]) and for the complexes **2–6** are shown in Table S3.

The DFT structure optimizations yield for the N2–Li1–N3 angle in **1** values between 160.2° (BP86-D4/def2-TZVPP) and 169.6° (B3LYP/def2-TZVPP). The Fe–Li1 distance is predicted between 2.887 Å (B3LYP/def2-TZVPP) and 2.756 Å (BP86-D4/def2-TZVPP) (see Table S3), confirming the experimental value and validating the used methods. The tilt angle is calculated between 2.8 and 6.1°, while the calculated torsion angle in the amidinate substituents ranges from 72.4 to 76.3° (cf. Table S3), which represents approximately 6° of difference with the experimental value obtained in the solid phase.

Confirming the experimental results, calculations indicate a retention of the almost linear N3–Cu2–N2 configuration in **2**. The values for the tilt angle are also in good agreement with those found in the X-ray analysis being around 6.4–8.4° (See Table S3).^{53,63} For **3**, the torsion and tilt angles were predicted between 66.1 and 71.5° and 9.8 and 11.9°, respectively. In general, optimized geometries for **2** and **3** are in an overall good agreement with the experimental values.^{64–66} The experimental observation of different stabilities of **2** and **3** (see previous sections) was also confirmed at the BP86/def2-SV(P) level of theory by analyzing the relative stability of the two complexes when Ag/Cu are exchanged, see Figure 6.^{67–70}

For the “ansa” type structure **4**, the Fe–Cu1 distance is predicted to be slightly longer than in **2**, ranging between 3.185 and 3.224 Å. Also, in contrast to **2**, the Cp–Cp’ tilt and N2–Cu1–N3 angles are reduced approximately by 3–4° when dispersion interactions using the models D3(BJ) and D4 are considered, which improves agreement with experiments.

Selected structural parameters for **5** and **6** are also included in Table S3. Although both complexes were optimized without symmetry constraints, the resulting structures agree with a C_i symmetry. Given that silver has an atomic radius close to that or even a bit larger than gold, theoretical values for bond lengths involving gold meet expectations with being within the same range or rather slightly shorter than those for **5**.^{71,72} For the angle between the Ph₃P unit, the metal (M: Ag, Au), and the amidinate group (N1–M–P), the optimized values are close to the experimental ones mirroring the ca. 10° wider angle obtained for gold.

In the four “ansa” type structures discussed (**1–4**), the inclusion of long-range interactions through the D3(BJ) and D4 models does not significantly affect the Cp–Cp’ tilt angle and when they do, they cause reductions in the order of 2–3°. Moreover, the Fe–M distances, with the exception of

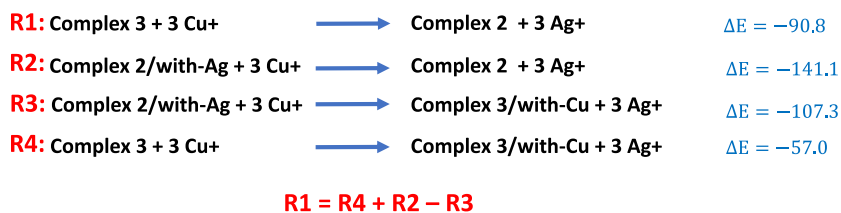


Figure 6. Analysis of the relative stabilities of complexes **2** and **3** via the reaction energies of the hypothetical Ag to Cu substitution reactions at the BP86/def2-SV(P) level of theory without zero-point vibrational corrections. All structures have been fully relaxed. /with-Ag and /with-Cu refer to complexes, in which Cu has been replaced with Ag or Ag has been replaced with Cu, respectively (units: kcal·mol^{−1}).

Table 1. Dispersion Interaction Energies [kcal mol⁻¹] of 2–6 Obtained Using the D3(BJ) Models for Structures Obtained with Six Different DFT Approaches in Conjunction with the def2-TZVPP Basis Set

		BP86	BP86-D3(BJ)	BP86-D4	B3LYP	B3LYP-D3(BJ)	B3LYP-D4
2	E[Fe...Cu2]	-1.01	-1.03	-1.02	-0.96	-0.97	-0.96
	E[Cu1-DIPP] ^a	-6.56	-5.96	-6.10	-5.86	-5.91	-6.09
	E[Cu3A-DIPP] ^b	-6.02	-6.22	-6.30	-5.32	-5.71	-5.78
3	E[Fe...Ag1]	-1.22	-1.23	-1.22	-1.15	-1.15	-1.14
	E[Ag2-DIPP] ^c	-7.41	-7.52	-7.62	-6.62	-7.06	-7.18
	E[Ag2'-DIPP] ^d	-7.50	-7.97	-8.00	-6.68	-7.29	-7.37
4	E[Fe...Cu1]	-1.01	-1.00	-1.00	-0.96	-0.95	-0.095
	E[Cu2-DIPP] ^e	-6.32	-6.81	-6.74	-5.34	-6.08	-6.20
5	E[Ag-DIPP] ^f	-6.55	-7.39	-7.42	-5.77	-6.75	-6.88
6	E[Au-DIPP] ^f	-6.74	-8.50	-8.37	-5.73	-6.08	-6.08

^aDIPP moiety associated with the C19 carbon, see for example, Figure 3, complex 2. ^bDIPP moiety associated with the C49 carbon, see Figure 3, complex 2. ^cDIPP moiety associated with the C19 carbon, see for example, Figure 3, complex 3. ^dThe quasi-transparent Li(thf)₃ moiety of 3 (Figure 3) indicates that the corresponding groups are half occupied in the solid phase. This would correspond to an asymmetric structure in the gas phase as used for the computations, where the Li(thf)₃ group is only present on one side. This explains the asymmetry of the structure and the different values tabulated for the groups labeled with and without prime. (See Section 3 from Supporting Information). ^eDIPP moiety associated with the C37 carbon, see Figure 4, complex 4. ^fDIPP moiety associated with the C19/C19' carbon, see Figure 4. As discussed in the text, the gas-phase structures of complexes 5 and 6 used in the computations belong to the symmetry point group C_v, and therefore, the molecular groups with the same numbering but with prime are equivalent due to symmetry.

proligand-anion [Fc(NCN^{DIPP})₂Li]⁻, increase slightly when dispersive effects are taken into account (see Table S3).

These two geometric parameters therefore indicate that at least with the dispersion models used here, the Fe-M interaction does not represent the main reason of stabilization of these complexes. These last two facts together with the π-metal interactions observed experimentally in complexes 2–6 (Figures 3–4) led us to make a detailed analysis of the most important London dispersion forces [D3(BJ) model]. The results in this regard are reported in Table 1. In 2 and 3, it is observed that the long-range London interactions Cu1-DIPP and Cu3A-DIPP for 2 and Ag2-DIPP and Ag2'-DIPP for 3 are quantitatively more important than those between ferrocenic-Fe and Cu2 (2) and Fe and Ag1 (3). Furthermore, it is observed that while the Fe-Cu (2) and Fe-Ag (3) interaction energies remain practically constant regardless of whether or not dispersive corrections are considered in the structural determinations, this is not the case for the Cu- and Ag-DIPP interactions. Their dispersion energy increases progressively with geometries obtained with the D3(BJ) and D4 models. Similar results are observed in complex 4 when the interaction Fe-Cu1 is compared with those between the other metal, that is, Cu2, and the phenyl group close to it. In the case of complexes with non-bridged configuration, that is, complexes 5 and 6, it is observed that the molecular configuration stabilizes mainly because of the interaction of one of the DIPP groups (see Table 1 and Figure 4) with the metal Ag (5) or Au (6) that are in adjacent positions.

CONCLUSIONS

In this work, a combined synthetic and theoretical study on the coordination chemistry of a bulky bisamidate ferrocene ligand toward Li, Cu, Ag, and Au was carried out. A total of six complexes were synthesized, out of which four were found to feature an “ansa” type coordination motif (1–4) and two an opposite orientation of substituents (5 and 6). Intrigued by short Fe-M distances found in the molecular structures of 1–4, possible long-range interactions stabilizing the formation of complexes with bridged versus non-bridged structures were analyzed. Although London dispersion forces show a small

reciprocal interaction between Fe and M, the interactions of the DIPP groups with M and M' (M' ≠ Fe, M) are decisive for the stabilization of the bridged motif. Thus, contrasting to previously reported results,⁶³ neither the tilt angle nor the Fe...M distance was a clear indicator for a Fe → M electron-donor effect in the studied systems. This distinct conclusion was attributed to the different ligand system comprising various aromatic units. The latter results were experimentally visible via short π-M distances (M = Cu, Ag, Au) in all compounds and confirmed by theoretical estimates. With this work, we hope to have contributed to a better understanding of the stabilization of ferrocene-bridged compounds, the crucial influence of (long-range) dispersion forces, and the interpretation of short Fe-M distances as highly depending on the surrounding ligand system.

EXPERIMENTAL SECTION⁵⁰

Theoretical Methods. The structures of the complexes synthesized in this work were determined via DFT by the BP86⁶⁷ and B3LYP⁷³ functionals in conjunction with the def2-TZVPP basis set.⁶⁹ All the calculations were performed employing the TURBOMOLE program package.⁷⁴ The resolution of identity approximation was applied in all the cases.^{75,76} A self-consistent-field convergence threshold of 10⁻⁸ E_h and a geometry convergence energy threshold of 10⁻⁶ E_h for the total energy and of 10⁻⁵ E_h a₀⁻¹ for the Cartesian gradient were used. The numerical quadrature was performed using a spherical grid 5 as defined in the TURBOMOLE program.⁷⁷ Dispersion effects on the molecular structure were investigated by incorporating in the DFT calculations the dispersion correction model D3 with Becke-Johnson damping D3(BJ)^{78,79} as well as the correction termed D4.^{79–81} A detailed analysis of the London dispersion interaction was carried out by using the program DFT-D3 of Grimme et al.^{78,79} The xyz-coordinates of the optimized structures analyzed in this work are provided in the Supporting Information.

General Methods and Instruments. The common Schlenk technique was applied to carry out all reactions under an inert atmosphere using a dual-manifold Schlenk line (inert gas: N₂, vacuum up to 1·10⁻³ mbar) or an MBraun glovebox (argon atmosphere). All reactions containing silver and gold

were handled under exclusion of light as a precaution (use of common aluminum films). Dry solvents were stored under a nitrogen atmosphere in Schlenk flasks. They were obtained using a MBraun SPS-800 solvent purification system (diethyl ether, toluene, and *n*-pentane) or by distillation over potassium (THF) or P₂O₅ (CH₂Cl₂). Deuterated solvents were purchased from commercial sources and dried over the NaK alloy (C₆D₆ and THF-*d*₈). The dilithioferrocene TMEDA adduct [FcLi₂(TMEDA)_{2/3}],^{82,83} [CuCl(Ph₃P)],⁸⁴ [AgCl(Ph₃P)],⁸⁴ and [AuCl(Ph₃P)]⁸⁵ were prepared following literature procedures. All other chemicals were obtained from commercial sources and used as received.

A Bruker AVANCE 400 MHz, AVANCE III 300 MHz, or AVANCE III 400 MHz was used to record NMR spectra. Chemical shifts are given in parts per million (ppm), referenced to the remaining ¹H/¹³C signal of the solvent used⁸⁶ and reported relative to tetramethylsilane. Resonance multiplicities are abbreviated as the following: s = singlet, d = doublet, t = triplet, q = quartet, bs = broad singlet, m = multiplet. Further assignment was done with the following: Cp = cyclopentadienyl, Ar = aromatic. If not stated otherwise, all NMR spectra were obtained at 298 K.

IR spectra were recorded on a Bruker Tensor 37 equipped with a DLaTGS detector and a diamond ATR (attenuated total reflection) unit as well as a nitrogen flushed chamber.

For ESI mass spectrometry, a LTQ Orbitrap XL Q Exactive mass spectrometer (Thermo Fisher Scientific, San Jose, CA, USA) equipped with a HESI II probe was used. The instrument was calibrated in the *m/z* range 74–1822 using premixed calibration solutions (Thermo Scientific).

Elemental analyses were carried out on a Vario MICRO cube instrument from Elementar Analysensysteme GmbH.

All crystals used for single-crystal diffraction analysis were taken from the crystallization mother liquor and directly transferred into mineral oil. The remaining crystals were isolated from the mother liquor by decantation, dried under reduced pressure, and used to carry out further analytics. All yields given hence refer to crystalline samples to ensure the best possible purity of all compounds. Therefore, yields are generally lower compared to bulk isolation.

[Fc(NCN^{DIPP})₂Li][Li(thf)₄] (1). The dilithioferrocene TMEDA adduct (1.00 g, 3.62 mmol, 1.00 equiv) and bis(2,6-diisopropylphenyl)carbodiimide (2.62 g, 7.23 mmol, 2.00 equiv) were suspended in 30 mL of THF and stirred overnight at room temperature. The obtained orange suspension was heated (~80 °C) until a clear solution was formed. Subsequent storing at room temperature overnight resulted in an orange crystalline product, which was isolated by decantation and dried for several hours at elevated temperature (~50 °C). Yield: 1.22 g, 12.2 mmol, 34%; one molecule of THF remaining). The yield can be improved by reconcentrating the decanted mother liquor after every crystal isolation.

Depending on the drying time (and if heating is applied or not), the THF content of the obtained product varies.

¹H NMR (400 MHz, DMSO-*d*₆): δ (ppm) = 6.69 (d, ³J_{H,H} = 7.4 Hz, 8H, H^{Ar,m}), 6.43 (t, ³J_{H,H} = 7.4 Hz, 4H, H^{Ar,o}), 3.99 (s, 4H, H^{Cp}), 3.82 (s, 4H, H^{Cp}), 3.64–3.56 (m, 8H, MeCHMe), 0.96 (bs, 48H, CH₃)—¹H NMR (213 K, 400 MHz, THF-*d*₈): δ (ppm) = 6.98–6.87 (m, 2H, H^{Ar}), 6.83–6.74 (m, 4H, H^{Ar}), 6.72–6.65 (m, 2H, H^{Ar}), 6.63–6.57 (m, 2H, H^{Ar}), 6.54–6.47 (m, 2H, H^{Ar}), 4.61 (bs, 2H, H^{Cp}), 4.02 (bs, 2H, H^{Cp}), 3.92–3.83 (m, 2H, H^{Cp}), 3.84–3.74 (m, 2H, MeCHMe), 3.54–3.38 (m, 4H, MeCHMe), 3.20 (bs, 2H, H^{Cp}), 2.88–2.73 (m, 2H,

MeCHMe), 1.48–1.22 (m, CH₃^a), 1.32–1.22 (m, 6H, CH₃), 1.16–0.97 (m, CH₃^a), 0.97–0.80 (m, 6H, CH₃), 0.68 (d, ³J_{H,H} = 6.6 Hz, 6H, CH₃), 0.34 (d, ³J_{H,H} = 6.8 Hz, 6H, CH₃)—¹³C{¹H} NMR (75 MHz, THF-*d*₈): δ (ppm) = 158.3 (C_q), 152.9 (C_q), 150.7 (C_q), 143.4 (C_q), 125.9 (HC^{Ar}), 124.1 (HC^{Ar}), 122.1 (HC^{Ar}), 121.3 (HC^{Ar}), 118.8 (HC^{Ar}), 88.1 (C_q), 74.5 (HC), 65.5 (HC), 30.1^b, 28.4^b, 27.5^b, 23.6^b—MS (ESI): *m/z* (%) = 909.550 ([M-Li + H]⁺ cal. 909.549)—IR (ATR): $\tilde{\nu}$ (cm⁻¹) = 2958 (vs), 2865 (m), 1607 (w), 1586 (w), 1522 (s), 1486 (s), 1465 (m), 1432 (s), 1388 (w), 1359 (m), 1315 (m), 1241 (w), 1188 (vw), 1136 (vw), 1099 (vw), 1033 (w), 900 (w), 757 (m), 460 (vw)—EA: C₇₆H₁₀₈FeLi₂N₄O₄: calc. C 75.35; H 8.99; N 4.62; exp. C 75.42; H 7.89; N 4.76.

[Fc(NCN^{DIPP})₂Cu(CuCl)₂Li(thf)₃] (2). Fc(NCN^{DIPP}Li)₂·4THF (1) (150 mg, 124 μmol, 1.00 equiv) and CuCl (37.0 mg, 371 μmol, 3.00 equiv) were suspended in 10 mL of THF and stirred at room temperature overnight. Filtration through a syringe filter yielded an orange solution which was concentrated to ~4 mL. Subsequent gas diffusion of *n*-pentane in the solution yielded the product as orange crystals in a yield of 21% (36.0 mg, 25.8 μmol, contains three molecules of THF).

MS (ESI): *m/z* (%) = 1169.267 ([M-(Li(THF)₃)]⁻ cal. 1169.266)—IR (ATR): $\tilde{\nu}$ (cm⁻¹) = 3610 (vw), 2959 (vs), 2922 (w), 2862 (w), 1628 (vs), 1576 (w), 1541 (vs), 1505 (vs), 1493 (vs), 1463 (m), 1436 (s), 1397 (w), 1381 (w), 1360 (w), 1318 (w), 1257 (w), 1245 (w), 1209 (vw), 1190 (w), 1178 (vw), 1104 (vw), 1044 (w), 1027 (w), 977 (vw), 933 (vw), 905 (w), 824 (w), 803 (w), 781 (w), 766 (w), 731 (vw), 478 (w), 424 (vw)—EA: C₇₂H₁₀₀Cl₂Cu₃FeLiN₄O₃: calc. C 62.04; H 7.23; N 4.02; exp. C 62.21; H 6.21; N 4.28.

Once in the solid (crystalline) state the product showed very low solubility in THF and decomposition in acetonitrile. Therefore, no useful NMR spectra were obtained.

[Fc(NCN^{DIPP})₂Ag(AgCl)₂Li(thf)₃] (3). Fc(NCN^{DIPP}Li)₂·4THF (1) (150 mg, 124 μmol, 1.00 equiv) and AgCl (53.2 mg, 371 μmol, 3.00 equiv) were stirred overnight in 10 mL of THF in the dark. The obtained orange suspension was filtered via a syringe filter and concentrated to ~4 mL, and *n*-pentane was diffused into it. Compound 3 was isolated as orange-red crystals (48.2 mg, 32.3 μmol, 26% calculated with three molecules of THF left). Please note that 3 shows limited stability in its mother liquor as well and slowly decomposes/forms a gray precipitate (probably Ag⁰), also when kept under exclusion of light.

IR (ATR): $\tilde{\nu}$ (cm⁻¹) = 3055 (vw), 2958 (vs), 2921 (m), 2865 (m), 1635 (vw), 1572 (vw), 1497 (vs), 1488 (vs), 1462 (s), 1435 (m), 1397 (w), 1381 (w), 1368 (w), 1359 (w), 1317 (w), 1256 (vw), 1242 (w), 1209 (vw), 1189 (vw), 1177 (vw), 1144 (vw), 1100 (vw), 1057 (w), 1046 (w), 1031 (w), 961 (vw), 933 (vw), 899 (w), 828 (vw), 802 (w), 782 (vw), 767 (w), 726 (vw), 519 (vw), 469 (w), 417 (vw). EA: C₇₂H₁₀₀Cl₂Ag₃FeLiN₄O₃: calc. C 56.64; H 6.60; N 3.67; exp. C 56.27; H 6.15; N 3.80.

Once in the solid (crystalline) state the product showed very low solubility in THF and decomposition (also in the mother liquor if kept too long). Therefore, no NMR spectra could be obtained.

[Fc(NCN^{DIPP})₂Cu(CuPPh₃)] (4). Fc(NCN^{DIPP}Li)₂·1THF (1) (100 mg, 101 μmol, 1.00 equiv) and 72.6 mg of [CuCl(PPh₃)] (201 μmol, 2.00 equiv) were stirred in 10 mL of THF at 70 °C over 3 days. After removing the solvent from the yellow-orange suspension, the solid residues were extracted with 8 mL of dichloromethane. After filtration (syringe filter), the solvent was removed to dryness and the resulting residues

dissolved in 4 mL of THF. Gas diffusion of *n*-pentane into the solution yielded **3** as orange crystals (72.6 mg, 50.3 μ mol, 50% calculated including one molecule of THF and *n*-pentane each).

Note: if crystallization is maintained for too long, a white precipitate is formed (probably PPh₃). However, if the flask is shaken vigorously, the solid suspends and the crystals (stay on the bottom of the flask) may be isolated by decantation.

¹H NMR (223 K, 400 MHz, THF-*d*₈): δ (ppm) = 7.53–7.47 (m, 1H, HAr^{DIPP}), 7.47–7.40 (m, 3H, H^{Ph}), 7.31–7.24 (m, 6H, H^{Ph}), 7.21–6.91 (m, 5H, HAr^{DIPP}), 6.91–6.83 (m, 6H, H^{Ph}), 6.83–6.77 (m, 3H, HAr^{DIPP}), 6.61–6.51 (m, 2H, HAr^{DIPP}), 6.48 (t, ³J_{H,H} = 7.7 Hz, 1H, HAr^{DIPP}), 5.53–5.43 (m, 1H, H^{Cp1}), 5.30–5.21 (m, 1H, H^{Cp2}), 4.49–4.36 (m, 1H, H^{Cp1}), 4.35–4.26 (m, 1H, H^{Cp2}), 3.90–3.84 (m, 1H, H^{Cp1}), 3.81–3.77 (m, 1H, H^{Cp2}), 3.50–3.46 (m, 1H, H^{Cp2}), 3.46–3.43 (m, 1H, H^{Cp1}), 3.42–3.32 (m, 1H, H₃CCHCH₃), 2.87–2.66 (m, 2H, H₃CCHCH₃), 1.66–1.53 (m, 9H, CH₃), 1.45 (d, ³J_{H,H} = 6.8 Hz, 6H, CH₃), 1.40 (d, ³J_{H,H} = 6.6 Hz, 3H, CH₃), 1.36–1.20 (m, CH₂Pentan + CH₃), 1.09 (d, ³J_{H,H} = 7.0 Hz, 3H, CH₃), 1.02 (d, ³J_{H,H} = 7.0 Hz, 3H, CH₃), 0.81–0.74 (m, 6H, CH₃), 0.67 (d, ³J_{H,H} = 6.5 Hz, 3H, CH₃), 0.63 (d, ³J_{H,H} = 6.5 Hz, 3H, CH₃), 0.56 (d, ³J_{H,H} = 6.8 Hz, 3H, CH₃), 0.50 (d, ³J_{H,H} = 6.7 Hz, 3H, CH₃), 0.35 (d, ³J_{H,H} = 6.8 Hz, 3H)—³¹P{¹H} NMR (162 MHz, THF-*d*₈): δ (ppm) = 8.3 (s)—¹³C{¹H} NMR (101 MHz, THF-*d*₈): δ (ppm) = 170.7 (d, ¹J_{C,P} = 3.9 Hz, C_q), 159.1 (C_q), 151.5 (C_q), 148.1 (C_q), 146.5 (C_q), 143.2 (C_q), 141.4 (C_q), 135.0 (HC^{Ar}), 134.8 (HC^{Ar}), 134.7 (HC^{Ar}), 134.5 (HC^{Ar}), 131.7 (d, J_{C,P} = 2.0 Hz, HC^{Ar}), 130.9 (C_q), 130.5 (C_q), 129.7 (HC^{Ar}), 129.5 (HC^{Ar}), 129.5 (HC^{Ar}), 129.4 (HC^{Ar}), 129.3 (HC^{Ar}), 129.3 (HC^{Ar}), 126.3 (HC^{Ar}), 125.4 (HC^{Ar}), 123.2 (HC^{Ar}), 119.9 (HC^{Ar}), 89.9 (C_q), 84.8 (C_q), 74.3 (HC^{Cp}), 73.7 (HC^{Cp}), 73.4 (HC^{Cp}), 71.5 (HC^{Cp}), 70.5 (HC^{Cp}), 70.0 (HC^{Cp}), 69.0 (HC^{Cp}), 68.3 (HC^{Cp}), 68.0 (HC^{Cp}), 67.8 (HC^{Cp}), 67.8 (HC^{Cp}), 67.6 (HC^{Cp}), 29.6–27.9 (H₃CCHCH₃), 25.7–23.6 (CH₃), 25.9 (CH₃), 25.7 (CH₃), 25.5 (CH₃)—MS (ESI): *m/z* (%) = 1299.501 ([M + H]⁺ cal. 1299.498), 1235.577 ([M–Cu+2H]⁺ cal. 1235.578), 973.486 ([M–CuPPh₃+2H]⁺ cal. 973.487)—IR (ATR): $\tilde{\nu}$ (cm⁻¹) = 3053 (vw), 2958 (vs), 2862 (m), 1614 (vw), 1587 (vw), 1531 (s), 1489 (vs), 1464 (m), 1435 (s), 1383 (w), 1358 (w), 1314 (m), 1242 (w), 1211 (vw), 1190 (vw), 1136 (vw), 1099 (m), 1034 (vw), 977 (vw), 904 (vw), 822 (vw), 802 (vw), 780 (w), 760 (w), 745 (m), 695 (m), 531 (w), 517 (vw), 504 (m), 490 (vw), 473 (w), 426 (vw)—EA: C₈₂H₉₉N₄Cu₂PFeO (incl. 1 THF): calc. C 71.86; H 7.28; N 4.09; exp. C 71.15; H 6.82; N 4.03.

Due to overlay with H^{Cp} and solvent resonances, not all CH₃CHCH₃ resonances could be identified unambiguously. The ³¹P{¹H} spectrum showed small impurities (~5%). ¹³C{¹H}: not all resonances could be detected or assigned due to dynamics at room temperature and overlay of numerous resonances.

[Fc(NCN^{DIPP}AgPPh₃)₂] (**5**). Fc(NCN^{DIPP}Li)₂1THF (**1**) (100 mg, 101 μ mol, 1.00 equiv) and 81.5 mg of [AgCl(PPh₃)] (201 μ mol, 2.00 equiv) were suspended in 10 mL of THF and stirred over 3 days at room temperature in the dark. After removal of the solvent, the orange solids were extracted with 8 mL of dichloromethane. After filtration (PTFE syringe filter) and drying under reduced pressure, the orange residues were dissolved in 4 mL of THF. Gas diffusion of *n*-pentane into the latter yielded the product as yellow-orange crystals (91.5 mg, 53.1 μ mol, 53% calc. with one molecule left inside the product).

Please note that when kept too long in their mother liquor, a grayish precipitate forms. However, the product can be isolated

by suspending the precipitate (e.g., in the mother liquor or *n*-pentane), followed by decantation (the crystalline product stays behind). Moreover, the product is thermally unstable and heating leads to decomposition.

¹H NMR (400 MHz, THF-*d*₈): δ (ppm) = 7.50–6.39 (m, H^{DIPP} + H^{Phenyl}), 4.34 (t, J_{H,H} = 1.9 Hz, 2H, H^{Cp}), 4.21 (t, J_{H,H} = 1.9 Hz, 2H, H^{Cp}), 4.12 (t, J_{H,H} = 1.9 Hz, 2H, H^{Cp}), 3.99 (t, J_{H,H} = 1.9 Hz, 2H, H^{Cp}), 3.56–3.46 (m, MeCHMe), 3.33–3.18* (m, MeCHMe), 3.14–3.01 (m, 2H, MeCHMe), 1.33^c (d, ³J_{H,H} = 6.9 Hz, CH₃), 1.28^c (d, ³J_{H,H} = 7.0 Hz, CH₃), 1.01^d (d, ³J_{H,H} = 6.8 Hz, CH₃), 0.92^d (superposition of two doublets CH₃), 0.89^c (d, ³J_{H,H} = 6.7 Hz, CH₃), 0.71 (d, ³J_{H,H} = 6.8 Hz, 6H, CH₃)—³¹P{¹H} NMR (162 MHz, THF-*d*₈): δ (ppm) = 15.7 (d, ¹J_{P,107Ag} = 578.3 Hz + d, ¹J_{P,109Ag} = 667.8 Hz)—¹³C{¹H, ³¹P(18.4 ppm)} NMR (101 MHz, THF-*d*₈): δ (ppm) = 161.4 (C_q), 161.3 (C_q), 156.2 (C_q), 150.2 (C_q), 148.8 (C_q), 148.6 (C_q), 148.4 (C_q), 148.4 (C_q), 147.8 (C_q), 147.8 (C_q), 147.6 (C_q), 143.2 (C_q), 143.2 (C_q), 140.8 (C_q), 140.1 (C_q), 139.3 (C_q), 139.1 (C_q), 138.8 (C_q), 136.2 (C_q), 134.9 (HC^{Ar}), 134.8 (HC^{Ar}), 134.8 (HC^{Ar}), 134.7 (HC^{Ar}), 134.7 (HC^{Ar}), 132.1 (HC^{Ar}), 131.7 (HC^{Ar}), 131.2 (C_q), 131.2 (C_q), 129.9 (HC^{Ar}), 129.7 (HC^{Ar}), 129.4 (HC^{Ar}), 128.6 (HC^{Ar}), 128.4 (HC^{Ar}), 128.2 (HC^{Ar}), 127.9 (HC^{Ar}), 126.1 (HC^{Ar}), 124.2 (HC^{Ar}), 124.1 (HC^{Ar}), 123.9 (HC^{Ar}), 123.8 (HC^{Ar}), 123.7 (HC^{Ar}), 123.7 (HC^{Ar}), 123.4 (HC^{Ar}), 123.3 (HC^{Ar}), 123.2 (HC^{Ar}), 123.0 (HC^{Ar}), 122.6 (HC^{Ar}), 122.4 (HC^{Ar}), 122.2 (HC^{Ar}), 122.1 (HC^{Ar}), 87.1 (C_q), 87.1 (C_q), 78.9 (C_q), 74.3 (HC^{Cp}), 73.7* (HC), 73.4* (HC), 71.8* (HC), 71.5* (HC), 70.7* (HC), 70.0* (HC), 69.4 (HC^{Cp}), 68.2 (HC^{Cp}), 29.6* (HC), 29.4* (HC), 29.2 (MeCHMe), 29.1* (HC), 28.8 (MeCHMe), 28.3* (HC), 28.1* (HC), 28.0 (MeCHMe), 25.9 (CH₃), 25.7 (CH₃), 25.5 (CH₃), 25.1 (CH₃), 24.9 (CH₃), 24.2 (CH₃), 24.2* (CH₃), 23.7 (CH₃)—MS (ESI): *m/z* (%) = 1649.545 ([M]⁺ cal. 1649.537), 1387.451 ([M–PPh₃ + H]⁺ cal. 1387.450), 1279.553 ([M–AgPPh₃+2H]⁺ cal. 1279.553)—IR (ATR): $\tilde{\nu}$ (cm⁻¹) = 3055 (vw), 2958 (vs), 2863 (m), 1611 (m), 1585 (w), 1510 (m), 1489 (m), 1463 (m), 1435 (m), 1380 (w), 1356 (w), 1316 (w), 1293 (vw), 1234 (vw), 1182 (w), 1132 (vw), 1100 (w), 1068 (vw), 1035 (vw), 891 (vw), 828 (vw), 801 (vw), 762 (m), 743 (m), 693 (m), 517 (m), 489 (m)—EA: C₉₆H₁₀₆N₄Ag₂P₂Fe: calc. C 69.91; H 6.48; N 3.40; exp. C 69.89; H 6.31; N 3.80.

c/d: A high baseline/overlaps did not allow reliable integration. Assignment was done with the help of ¹H COSY NMR spectroscopy.

Resonances for a second compound (possibly due to degradation) are visible, especially within the area of Cp protons (δ = 4.5–3.95 ppm) and in ³¹P{¹H} NMR spectroscopy. It shows very similar chemical shifts and patterns (marked with # in Figure S24) to the product. The percentage is estimated to <10%. Resonances tentatively assigned to the side/degradation product are marked with *. Due to overlaying of multiple resonances, no integrals could be determined within the aromatic region. For better visibility, only ¹³C{¹H, ³¹P} is given. The biproduct/other structure/decomposition also leads to more resonances than expected. An assignment whose resonances belong to the main product was not possible. Where possible, the estimated non-product resonances are marked with *.

[Fc(NCN^{DIPP}AuPPh₃)₂] (**6**). Fc(NCN^{DIPP}Li)₂1THF (**1**) (100 mg, 101 μ mol, 1.00 equiv) was stirred with 99.4 mg of [(AuCl)PPh₃] (201 μ mol, 2.00 equiv) in 10 mL of toluene at room temperature for 3 days. The yellow suspension was slightly

warmed and filtered (syringe filter). Gas diffusion of *n*-pentane into the solution or cooling of the concentrated solution yielded **6** as yellow crystals (57.2 mg, 28.44 μ mol, 28% including two molecules of toluene).

MS (ESI): m/z (%) = 1828.669 ($[M + H]^+$ cal. 1828.668), 1369.613 ($[M - AuPPh_3 + 2H]^+$ cal. 1369.615)—IR (ATR): $\tilde{\nu}$ (cm^{-1}) = 3054 (wv), 2958 (vs), 2923 (m), 2899 (w), 2864 (m), 1610 (w), 1585 (vw), 1548 (m), 1523 (m), 1504 (w), 1462 (m), 1436 (vs), 1379 (w), 1347 (m), 1330 (w), 1316 (m), 1293 (w), 1256 (w), 1237 (w), 1183 (w), 1101 (m), 891 (vw), 813 (vw), 800 (vw), 762 (w), 743 (m), 727 (w), 711 (w), 693 (m), 543 (m), 511 (m), 497 (m), 464 (w).

Elemental analysis gave consequently wrong carbon values; therefore, elemental composition was confirmed via HRMS. Due to very low solubility and low stability, no useful NMR spectra were obtained. Additionally, the product is thermally unstable and longer heating leads to decomposition. Reaction in THF however was not possible due to immediate decomposition.

■ ASSOCIATED CONTENT

SI Supporting Information

The Supporting Information is available free of charge at <https://pubs.acs.org/doi/10.1021/acsomega.1c07036>.

Spectra of compounds **1–6**; X-ray crystallographic studies; and theoretical calculations (PDF)

Crystallographic data of **1** (CIF)

Crystallographic data of **2** (CIF)

Crystallographic data of **3** (CIF)

Crystallographic data of **5** (CIF)

Crystallographic data of **6** (CIF)

■ AUTHOR INFORMATION

Corresponding Authors

Juana Vázquez Quesada – Institute of Physical Chemistry, Karlsruhe Institute of Technology (KIT), 76131 Karlsruhe, Germany; Email: juana.quesada@kit.edu

Peter W. Roesky – Institute of Inorganic Chemistry, Karlsruhe Institute of Technology (KIT), 76131 Karlsruhe, Germany; orcid.org/0000-0002-0915-3893; Email: roesky@kit.edu

Authors

Milena Dahlen – Institute of Inorganic Chemistry, Karlsruhe Institute of Technology (KIT), 76131 Karlsruhe, Germany

Luis Santos Correa – Institute of Inorganic Chemistry, Karlsruhe Institute of Technology (KIT), 76131 Karlsruhe, Germany; orcid.org/0000-0002-0365-0549

Luca Münzfeld – Institute of Inorganic Chemistry, Karlsruhe Institute of Technology (KIT), 76131 Karlsruhe, Germany; orcid.org/0000-0001-5678-8560

Niklas Reinfandt – Institute of Inorganic Chemistry, Karlsruhe Institute of Technology (KIT), 76131 Karlsruhe, Germany

Wim Klopper – Institute of Physical Chemistry, Karlsruhe Institute of Technology (KIT), 76131 Karlsruhe, Germany

Complete contact information is available at:

<https://pubs.acs.org/doi/10.1021/acsomega.1c07036>

Notes

The authors declare no competing financial interest.

■ ACKNOWLEDGMENTS

W.K. and P.W.R. gratefully acknowledge support by the Deutsche Forschungsgemeinschaft (DFG) through the Trans-regional Collaborative Research Centre 88 [Cooperative Effects in Homo- and Heterometallic Complexes (3MET)], Projects C1 and C3. W.K. and J.V.Q. gratefully acknowledge support by the DFG through the Priority Program 1807 [Control of London Dispersion Interactions in Molecular Chemistry], Project KL 721/5-2. M.D. and N.R. thank Fonds der Chemischen Industrie for their fellowships (nos. 103581 and 102431).

■ ADDITIONAL NOTES

^aTwo overlaid resonances according to ¹H–COSY-NMR spectroscopy. Due to remaining dynamics with an elevated baseline, obtained integrals do not fit expected values.

^bResonances which probably belong to methyl group carbon atoms but do not appear in HMQC (due to dynamics) and can therefore not be assigned definitely. NMR spectra in THF-*d*₈ were recorded from a different batch which was not dried thoroughly and therefore contains more THF. Please note that **1** shows only limited stability in DMSO.

^cResonance corresponds to two methyl groups (six protons).

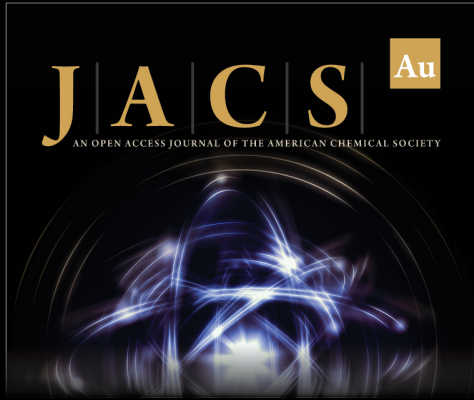
^dResonance corresponds to 4 methyl groups (12 protons).

■ REFERENCES


- (1) Kauffman, G. B. The discovery of ferrocene, the first sandwich compound. *J. Chem. Educ.* **1983**, *60*, 185.
- (2) Braga, S. S.; Silva, A. M. S. A New Age for Iron: Antitumoral Ferrocenes. *Organometallics* **2013**, *32*, 5626–5639.
- (3) Piotrowicz, M.; Zakrzewski, J. Aerobic Dehydrogenative Heck Reaction of Ferrocene with a Pd(OAc)₂/4,5-Diazafluoren-9-one Catalyst. *Organometallics* **2013**, *32*, 5709–5712.
- (4) Kumar, K.; Carrère-Kremer, S.; Kremer, L.; Guérardel, Y.; Biot, C.; Kumar, V. 1H-1,2,3-Triazole-Tethered Isatin–Ferrocene and Isatin–Ferrocenylchalcone Conjugates: Synthesis and in Vitro Antitubercular Evaluation. *Organometallics* **2013**, *32*, 5713–5719.
- (5) Elbert, J.; Gallei, M.; Rüttiger, C.; Brunsen, A.; Didzoleit, H.; Stühn, B.; Rehahn, M. Ferrocene Polymers for Switchable Surface Wettability. *Organometallics* **2013**, *32*, 5873–5878.
- (6) Kealy, T. J.; Pauson, P. L. A New Type of Organo-Iron Compound. *Nature* **1951**, *168*, 1039–1040.
- (7) Miller, S. A.; Tebboth, J. A.; Tremaine, J. F. 114. Dicyclopentadienyliron. *J. Chem. Soc.* **1952**, 632–635.
- (8) Fischer, E. O.; Pfab, W. Cyclopentadien-Metallkomplexe, ein neuer Typ metallorganischer Verbindungen. *Z. Naturforsch., B* **1952**, *7*, 377–379.
- (9) Wilkinson, G.; Rosenblum, M.; Whiting, M. C.; Woodward, R. B. The structure of iron bis-cyclopentadienyl. *J. Am. Chem. Soc.* **1952**, *74*, 2125–2126.
- (10) Gagne, R. R.; Koval, C. A.; Lisensky, G. C. Ferrocene as an internal standard for electrochemical measurements. *Inorg. Chem.* **1980**, *19*, 2854–2855.
- (11) Kameoka, A.; Tsuchiya, K. Influence of Ferrocene on Engine and Vehicle Performance. *SAE Technical Paper 2006-01-3448*, 2006.
- (12) Elwardany, A. E.; Marei, M. N.; Eldrainy, Y.; Ali, R. M.; Ismail, M.; El-kassaby, M. M. Improving performance and emissions characteristics of compression ignition engine: Effect of ferrocene nanoparticles to diesel-biodiesel blend. *Fuel* **2020**, *270*, 117574.
- (13) Fery-Forgues, S.; Delavaux-Nicot, B. Ferrocene and ferrocenyl derivatives in luminescent systems. *J. Photochem. Photobiol., A* **2000**, *132*, 137–159.
- (14) Cao, W.; Ferrance, J. P.; Demas, J.; Landers, J. P. Quenching of the Electrochemiluminescence of Tris(2,2'-bipyridine)ruthenium(II) by Ferrocene and Its Potential Application to Quantitative DNA Detection. *J. Am. Chem. Soc.* **2006**, *128*, 7572–7578.


- (15) Gan, J.; Tian, H.; Wang, Z.; Chen, K.; Hill, J.; Lane, P. A.; Rahn, M. D.; Fox, A. M.; Bradley, D. D. C. Synthesis and luminescence properties of novel ferrocene–naphthalimides dyads. *J. Organomet. Chem.* **2002**, *645*, 168–175.
- (16) Li, M.; Guo, Z.; Zhu, W.; Marken, F.; James, T. D. A redox-activated fluorescence switch based on a ferrocene–fluorophore–boronic ester conjugate. *Chem. Commun.* **2015**, *51*, 1293–1296.
- (17) Tropiano, M.; Kilah, N. L.; Morten, M.; Rahman, H.; Davis, J. J.; Beer, P. D.; Faulkner, S. Reversible Luminescence Switching of a Redox-Active Ferrocene–Europium Dyad. *J. Am. Chem. Soc.* **2011**, *133*, 11847–11849.
- (18) Wei, J.; Diaconescu, P. L. Redox-Switchable Ring-Opening Polymerization with Ferrocene Derivatives. *Acc. Chem. Res.* **2019**, *52*, 415–424.
- (19) Klenk, S.; Rupf, S.; Suntrup, L.; van der Meer, M.; Sarkar, B. The Power of Ferrocene, Mesoionic Carbenes, and Gold: Redox-Switchable Catalysis. *Organometallics* **2017**, *36*, 2026–2035.
- (20) Astruc, D. Why is Ferrocene so Exceptional? *Eur. J. Inorg. Chem.* **2017**, *2017*, 6–29.
- (21) Braunstein, P.; Carneiro, T. M. G.; Matt, D.; Balegrone, F.; Grandjean, D. β -Keto phosphines derived from ferrocene. Syntheses and structures of $[\text{Ph}_2\text{PCH}_2\text{C}(\text{O})(\eta^5\text{-C}_5\text{H}_4)\text{Fe}(\eta^5\text{-C}_5\text{H}_5)]$ (L') and trans- $[\text{PdCl}_2\text{L}^{12}]$. *J. Organomet. Chem.* **1989**, *367*, 117–132.
- (22) Bandoli, G.; Dolmella, A. Ligating ability of 1,1'-bis-(diphenylphosphino)ferrocene: a structural survey (1994–1998). *Coord. Chem. Rev.* **2000**, *209*, 161–196.
- (23) Ringenberg, M. R. Beyond Common Metal–Metal Bonds, κ -Bis(donor)ferrocenyl→Transition-Metal Interactions. *Chem.—Eur. J.* **2019**, *25*, 2396–2406.
- (24) Seyferth, D.; Hames, B. W.; Rucker, T. G.; Cowie, M.; Dickson, R. S. A novel palladium complex with iron-palladium dative bonding derived from 1,2,3-trithia[3]ferrocenophane, $(\text{Ph}_3\text{P})\text{PdFe}(\text{SC}_5\text{H}_4)_2 \cdot 0.5\text{C}_6\text{H}_5\text{CH}_3$. *Organometallics* **1983**, *2*, 472–474.
- (25) Akabori, S.; Kumagai, T.; Shirahige, T.; Sato, S.; Kawazoe, K.; Tamura, C.; Sato, M. Preparation of novel platinum and palladium complexes by reaction of 1,1'-metallocenedichalcogenols with tetrakis-(triphenylphosphine)palladium(0) or -platinum(0). The important role of the coordinating ability of the metal atom of the metallocene in product formation. *Organometallics* **1987**, *6*, 526–531.
- (26) Gramigna, K. M.; Oriá, J. V.; Mandell, C. L.; Tiedemann, M. A.; Dougherty, W. G.; Piro, N. A.; Kassel, W. S.; Chan, B. C.; Diaconescu, P. L.; Nataro, C. Palladium(II) and Platinum(II) Compounds of 1,1'-Bis(phosphino)metallocene (M = Fe, Ru) Ligands with Metal–Metal Interactions. *Organometallics* **2013**, *32*, 5966–5979.
- (27) Paretzki, A.; Pattacini, R.; Huebner, R.; Braunstein, P.; Sarkar, B. Stabilising a quinonoid-bridged dicopper(I) complex by use of a dpfp (dpfp = (diphenylphosphino)ferrocene) backbone. *Chem. Commun.* **2010**, *46*, 1497–1499.
- (28) Braunstein, P.; Bublin, D.; Sarkar, B. Synthesis of bis-(phosphinoferrocenyl) copper complexes from zwitterionic quinonoid ligands and their structural and redox properties. *Inorg. Chem.* **2009**, *48*, 2534–2540.
- (29) Canales, S.; Villacampa, M. D.; Laguna, A.; Gimeno, M. C. Coordination studies of the ferrocenyl phosphine selenide ligand $\text{FcCON}(\text{CH}_2\text{CH}_2\text{PPh}_2\text{Se})_2$. *J. Organomet. Chem.* **2014**, *760*, 84–88.
- (30) Junk, P. C.; Cole, M. L. Alkali-metal bis(aryl)formamidates: a study of coordinative versatility. *Chem. Commun.* **2007**, 1579–1590.
- (31) Edelmann, F. T. Lanthanide amidinates and guanidinates in catalysis and materials science: a continuing success story. *Chem. Soc. Rev.* **2012**, *41*, 7657–7672.
- (32) Kissounko, D. A.; Zabalov, M. V.; Brusova, G. P.; Lemenovskii, D. A. Principal trends in the chemistry of amidinate complexes of main-group and transition elements. *Russ. Chem. Rev.* **2006**, *75*, 351–374.
- (33) Edelmann, F. T. Lanthanide amidinates and guanidinates: from laboratory curiosities to efficient homogeneous catalysts and precursors for rare-earth oxide thin films. *Chem. Soc. Rev.* **2009**, *38*, 2253–2268.
- (34) Kaufmann, S.; Radius, M.; Moos, E.; Breher, F.; Roesky, P. W. Rhodium(I) and Iridium(I) Complexes of Ferrocenyl-Functionalized Amidinates and Bis(amidinates): $\kappa^2\text{N}$ -Coordination Versus Ferrocenyl Ortho-Metalation. *Organometallics* **2019**, *38*, 1721–1732.
- (35) Fichter, S.; Kaufmann, S.; Kaden, P.; Brunner, T. S.; Stumpf, T.; Roesky, P. W.; März, J. Cover Feature: Enantiomerically Pure Tetravalent Neptunium Amidinates: Synthesis and Characterization. *Chem.—Eur. J.* **2020**, *26*, 8832.
- (36) Coles, M. P. Application of neutral amidines and guanidines in coordination chemistry. *Dalton Trans.* **2006**, 985–1001.
- (37) Asay, M.; Jones, C.; Driess, M. N-heterocyclic carbene analogues with low-valent group 13 and group 14 elements: syntheses, structures, and reactivities of a new generation of multitailored ligands. *Chem. Rev.* **2011**, *111*, 354–396.
- (38) Kloditz, R.; Fichter, S.; Kaufmann, S.; Brunner, T. S.; Kaden, P.; Patzschke, M.; Stumpf, T.; Roesky, P. W.; Schmidt, M.; März, J. Series of Tetravalent Actinide Amidinates: Structure Determination and Bonding Analysis. *Inorg. Chem.* **2020**, *59*, 15670–15680.
- (39) Luo, Y.; Gao, Z.; Chen, J. Rare-earth metal bis(silylamide) complexes supported by ferrocene-substituted amidinate and their performance in cis-1,4 selective polymerization of isoprene. *J. Organomet. Chem.* **2017**, *846*, 18–23.
- (40) Multani, K.; Stanlake, L. J. E.; Stephan, D. W. Ti and Zr complexes of ferrocenyl amidinates. *Dalton Trans.* **2010**, *39*, 8957–8966.
- (41) Hagadorn, J. R.; Arnold, J. Ferrocene-Substituted Amidinate Derivatives: Syntheses and Crystal Structures of Lithium, Iron (II), and Cobalt (II) Complexes. *Inorg. Chem.* **1997**, *36*, 132–133.
- (42) Coles, M. P.; Stokes, F. A.; Kingsbury, B. F. K.; Day, B. M.; Hitchcock, P. B. Planar Chirality and Helical Polymers: Ferrocenyl-Substituted Amidinium–Carboxylate Salts. *Cryst. Growth Des.* **2011**, *11*, 3206–3212.
- (43) Kaufmann, S.; Roesky, P. W. Investigating a redox active samarium complex in catalytic reactions. *Eur. J. Inorg. Chem.* **2021**, *2021*, 2899.
- (44) Sato, M.; Katada, M.; Nakashima, S.; Sano, H.; Akabori, S. Syntheses and physicochemical properties of $\text{Cu}(\text{BF}_4)_2$ complexes of polythia[n]ferrocenophanes and the corresponding ferrocenium cations. *J. Chem. Soc., Dalton Trans.* **1990**, 1979–1984.
- (45) Herberhold, M.; Jin, G.-X.; Rheingold, A. L.; Sheats, G. F. Pentamethylcyclopentadienyl Halfsandwich Complexes of Rhodium and Iridium Containing 1,1'-Ferrocene Dichalcogenido Ligands. *Z. Naturforsch., B* **1992**, *47*, 1091–1098.
- (46) Braunstein, P.; Danopoulos, A. A. Transition Metal Chain Complexes Supported by Soft Donor Assembling Ligands. *Chem. Rev.* **2021**, *121*, 7346–7397.
- (47) Mirzadeh, N.; Privér, S. H.; Blake, A. J.; Schmidbaur, H.; Bhargava, S. K. Innovative Molecular Design Strategies in Materials Science Following the Auophilicity Concept. *Chem. Rev.* **2020**, *120*, 7551–7591.
- (48) Feuerstein, T. J.; Seifert, T. P.; Jung, A. P.; Müller, R.; Lebedkin, S.; Kappes, M. M.; Roesky, P. W. Efficient Blue Phosphorescence in Gold(I)-Acetylide Functionalized Coinage Metal Bis(amidinate) Complexes. *Chem.—Eur. J.* **2020**, *26*, 16676–16682.
- (49) Herrera, R. P.; Gimeno, M. C. Main Avenues in Gold Coordination Chemistry. *Chem. Rev.* **2021**, *121*, 8311–8363.
- (50) Dahlen, M. Systematischer Aufbau mehrkerniger Münzmetallkomplexe zur Untersuchung ihrer Lumineszenz und Synthese von d10-Ferrocenylbisamidinatkomplexen. Dissertation, Karlsruher Institut für Technologie (KIT), Göttingen, 2021.
- (51) Osako, T.; Tachi, Y.; Taki, M.; Fukuzumi, S.; Itoh, S. Modulation of Coordination Chemistry in Copper(I) Complexes Supported by Bis[2-(2-pyridyl)ethyl]amine-Based Tridentate Ligands. *Inorg. Chem.* **2001**, *40*, 6604–6609.
- (52) Pérez-Galán, P.; Delpont, N.; Herrero-Gómez, E.; Maseras, F.; Echavarren, A. M. Metal–Arene Interactions in Dialkylbiarylphosphane Complexes of Copper, Silver, and Gold. *Chem.—Eur. J.* **2010**, *16*, 5324–5332.
- (53) Nesmeyanov, A. N.; Struchkov, Y. T.; Sedova, N. N.; Andrianov, V. G.; Volgin, Y. V.; Sazonova, V. A. On the structure and properties of


- 2-copper-1-(dimethylaminomethyl)ferrocene. *J. Organomet. Chem.* **1977**, *137*, 217–221.
- (54) Alvarez, S. A cartography of the van der Waals territories. *Dalton Trans.* **2013**, *42*, 8617–8636.
- (55) Batsanov, S. S. Van der Waals Radii of Elements. *Inorg. Mater.* **2001**, *37*, 871–885.
- (56) Nesmeyanov, A. N.; Sedova, N. N.; Struchkov, Y. T.; Andrianov, V. G.; Stakheeva, E. N.; Sazonova, V. A. On the structure and properties of 2-silver-(dimethylaminomethyl)ferrocene. *J. Organomet. Chem.* **1978**, *153*, 115–122.
- (57) Pearson, R. G. Hard and soft acids and bases—the evolution of a chemical concept. *Coord. Chem. Rev.* **1990**, *100*, 403–425.
- (58) Pearson, R. G. Hard and Soft Acids and Bases. *J. Am. Chem. Soc.* **1963**, *85*, 3533–3539.
- (59) Green, J. C. Bent metallocenes revisited. *Chem. Soc. Rev.* **1998**, *27*, 263–272.
- (60) Musgrave, R. A.; Russell, A. D.; Manners, I. Strained Ferrocenophanes. *Organometallics* **2013**, *32*, 5654–5667.
- (61) Jess, K.; Baabe, D.; Bannenberg, T.; Brandhorst, K.; Freytag, M.; Jones, P. G.; Tamm, M. Ni–Fe and Pd–Fe Interactions in Nickel(II) and Palladium(II) Complexes of a Ferrocene-Bridged Bis(imidazolin-2-imine) Ligand. *Inorg. Chem.* **2015**, *54*, 12032–12045.
- (62) Green, A. G.; Kiesz, M. D.; Oria, J. V.; Elliott, A. G.; Buechler, A. K.; Hohenberger, J.; Meyer, K.; Zink, J. I.; Diaconescu, P. L. Characterization of an Iron–Ruthenium Interaction in a Ferrocene Diamide Complex. *Inorg. Chem.* **2013**, *52*, 5603–5610.
- (63) Stegner, P.; Färber, C.; Oetzel, J.; Siemeling, U.; Wiesinger, M.; Langer, J.; Pan, S.; Holzmann, N.; Frenking, G.; Albold, U.; Sarkar, B.; Harder, S. d–d Dative Bonding Between Iron and the Alkaline-Earth Metals Calcium, Strontium, and Barium. *Angew. Chem., Int. Ed.* **2020**, *59*, 14615–14620.
- (64) Li, Y.; Liu, Y.-Y.; Chen, X.-J.; Xiong, X.-H.; Li, F.-S. Synthesis, spectroscopic characterization, X-ray structure, and DFT calculations of some new 1,4-dihydro-2,6-dimethyl-3,5-pyridinedicarboxamides. *PLoS One* **2014**, *9*, No. e91361.
- (65) Riehn, C.; Degen, A.; Weichert, A.; Bolte, M.; Egert, E.; Brutschy, B.; Tarakeshwar, P.; Kim, K. S. Molecular Structure of p-Cyclohexylaniline. Comparison of Results Obtained by X-ray Diffraction with Gas Phase Laser Experiments and ab Initio Calculations. *J. Chem. Phys. A* **2000**, *104*, 11593–11600.
- (66) Domenicano, A. H. *István, Accurate Molecular Structures: Their Determination and Importance*; Oxford University Press: Oxford, 1992.
- (67) Becke, A. D. Density-functional exchange-energy approximation with correct asymptotic behavior. *Phys. Rev. A Gen. Phys.* **1988**, *38*, 3098–3100.
- (68) Gulde, R.; Pollak, P.; Weigend, F. Error-Balanced Segmented Contracted Basis Sets of Double-zeta to Quadruple-zeta Valence Quality for the Lanthanides. *J. Chem. Theory Comput.* **2012**, *8*, 4062–4068.
- (69) Weigend, F.; Ahlrichs, R. Balanced basis sets of split valence, triple zeta valence and quadruple zeta valence quality for H to Rn: Design and assessment of accuracy. *PCCP* **2005**, *7*, 3297–3305.
- (70) Weigend, F.; Häser, M.; Patzelt, H.; Ahlrichs, R. RI-MP2: optimized auxiliary basis sets and demonstration of efficiency. *Chem. Phys. Lett.* **1998**, *294*, 143–152.
- (71) Bayler, A.; Schier, A.; Bowmaker, G. A.; Schmidbaur, H. Gold Is Smaller than Silver. Crystal Structures of [Bis(trimesitylphosphine)-gold(I)] and [Bis(trimesitylphosphine)silver(I)] Tetrafluoroborate. *J. Am. Chem. Soc.* **1996**, *118*, 7006–7007.
- (72) Hollemann, A. F.; Wiberg, E.; Wiberg, N. *Lehrbuch der Anorganischen Chemie*, 102 ed.; de Gruyter, Berlin: 2007.
- (73) Becke, A. D. A new mixing of Hartree–Fock and local density-functional theories. *J. Chem. Phys.* **1993**, *98*, 1372–1377.
- (74) TURBOMOLE, V., A development of University of Karlsruhe and Forschungszentrum Karlsruhe GmbH, 1989–2007, TURBOMOLE GmbH, since 2007, available from <http://www.turbomole.com>.
- (75) Weigend, F. Accurate Coulomb-fitting basis sets for H to Rn. *Phys. Chem. Chem. Phys.* **2006**, *8*, 1057–1065.
- (76) Eichkorn, K.; Treutler, O.; Öhm, H.; Häser, M.; Ahlrichs, R. Auxiliary basis sets to approximate Coulomb potentials. *Chem. Phys. Lett.* **1995**, *240*, 283–290.
- (77) Treutler, O.; Ahlrichs, R. Efficient molecular numerical integration schemes. *J. Chem. Phys.* **1995**, *102*, 346–354.
- (78) Grimme, S.; Antony, J.; Ehrlich, S.; Krieg, H. A consistent and accurate ab initio parametrization of density functional dispersion correction (DFT-D) for the 94 elements H–Pu. *J. Chem. Phys.* **2010**, *132*, 154104.
- (79) Grimme, S.; Ehrlich, S.; Goerigk, L. Effect of the damping function in dispersion corrected density functional theory. *J. Comput. Chem.* **2011**, *32*, 1456–1465.
- (80) Caldeweyher, E.; Ehlert, S.; Hansen, A.; Neugebauer, H.; Spicher, S.; Bannwarth, C.; Grimme, S. A generally applicable atomic-charge dependent London dispersion correction. *J. Chem. Phys.* **2019**, *150*, 154122.
- (81) Caldeweyher, E.; Bannwarth, C.; Grimme, S. Extension of the D3 dispersion coefficient model. *J. Chem. Phys.* **2017**, *147*, 034112.
- (82) Bishop, J. J.; Davison, A.; Katcher, M. L.; Lichtenberg, D. W.; Merrill, R. E.; Smart, J. C. Symmetrically disubstituted ferrocenes: I. The synthesis of potential bidentate ligands. *J. Organomet. Chem.* **1971**, *27*, 241–249.
- (83) Butler, I. R.; Cullen, W. R.; Ni, J.; Rettig, S. J. The structure of the 3:2 adduct of 1,1'-dilithioferrocene with tetramethylethylenediamine. *Organometallics* **1985**, *4*, 2196–2201.
- (84) Halim, M.; Kennedy, R. D.; Suzuki, M.; Khan, S. I.; Diaconescu, P. L.; Rubin, Y. Complexes of Gold(I), Silver(I), and Copper(I) with Pentaaryl[60]fullerides. *J. Am. Chem. Soc.* **2011**, *133*, 6841–6851.
- (85) Price, G. A.; Brisdon, A. K.; Flower, K. R.; Pritchard, R. G.; Quayle, P. Solvent effects in gold-catalysed A3-coupling reactions. *Tetrahedron Lett.* **2014**, *55*, 151–154.
- (86) Fulmer, G. R.; Miller, A. J. M.; Sherden, N. H.; Gottlieb, H. E.; Nudelman, A.; Stoltz, B. M.; Bercaw, J. E.; Goldberg, K. I. NMR Chemical Shifts of Trace Impurities: Common Laboratory Solvents, Organics, and Gases in Deuterated Solvents Relevant to the Organometallic Chemist. *Organometallics* **2010**, *29*, 2176–2179.



JACS Au
AN OPEN ACCESS JOURNAL OF THE AMERICAN CHEMICAL SOCIETY

 Editor-in-Chief
Prof. Christopher W. Jones
Georgia Institute of Technology, USA

Open for Submissions 

pubs.acs.org/jacsau  ACS Publications
Most Trusted. Most Cited. Most Read.